



# Practical Charger Placement Scheme for Wireless Rechargeable Sensor Networks with Obstacles

WEI YOU, MEIXUAN REN, YUZHUO MA, DIE WU, and JILIN YANG, Sichuan Normal University, China

XUXUN LIU, South China University of Technology, China

TANG LIU, Sichuan Normal University, China

11

Benefitting from the maturation of Wireless Power Transfer technology, Wireless Rechargeable Sensor Networks have become a promising solution for prolonging network lifetime. In practical charging scenarios, obstacles are ubiquitous. However, most prior arts have failed to consider the combined impacts of the material, size, and location of obstacles on the charging performance, making these schemes unsuitable for real applications. In this article, we study a fundamental issue of Wireless chArger placement wIth obsTacles (WAIT), that is, how to place wireless chargers by comprehensively considering these parameters of obstacles, such that the overall charging utility is maximized. To tackle the WAIT problem, we first build a practical charging model with obstacles by introducing shadow fading, and conduct experiments to verify its correctness. Then, we design a piecewise constant function to approximate the nonlinear charging power. Afterwards, we develop a Dominating Coverage Set extraction algorithm to reduce the continuous solution space to a limited number. Finally, we prove the WAIT problem is a maximizing monotone submodular function problem, and propose a  $1 - 1/e - \epsilon$  approximation algorithm to address it. Extensive simulations and field experiments show that our scheme outperforms comparison algorithms by at least 20.6% in charging utility improvement.

CCS Concepts: • Computer systems organization → Sensor networks;

Additional Key Words and Phrases: Charger placement, wireless rechargeable sensor networks, obstacles

## ACM Reference format:

Wei You, Meixuan Ren, Yuzhuo Ma, Die Wu, Jilin Yang, Xuxun Liu, and Tang Liu. 2023. Practical Charger Placement Scheme for Wireless Rechargeable Sensor Networks with Obstacles. *ACM Trans. Sensor Netw.* 20, 1, Article 11 (October 2023), 23 pages.

<https://doi.org/10.1145/3614431>

This work is partially supported by the National Natural Science Foundation of China (Grants No. 62072320 and No. 62002250) and the Natural Science Foundation of Sichuan Province (Grants No. 2022NSFSC0569 and No. 2022NSFSC0929). Authors' addresses: W. You, M. Ren, Y. Ma, D. Wu, J. Yang, and T. Liu (corresponding author), Sichuan Normal University, Chengdu, 610101, China; Visual Computing and Virtual Reality Key Laboratory of Sichuan Province, Chengdu, 610068, China; emails: weiyou@stu.sicnu.edu.cn, meixuanren@stu.sicnu.edu.cn, yuzhuoma@stu.sicnu.edu.cn, wd@sicnu.edu.cn, jilinyang@sicnu.edu.cn, liutang@sicnu.edu.cn; X. Liu, South China University of Technology, Guangzhou, 510641, China; Key Laboratory of Autonomous Systems and Network Control; Ministry of Education of China, Guangzhou, 510641, China; email: liuxuxun@scut.edu.cn.

Permission to make digital or hard copies of all or part of this work for personal or classroom use is granted without fee provided that copies are not made or distributed for profit or commercial advantage and that copies bear this notice and the full citation on the first page. Copyrights for components of this work owned by others than the author(s) must be honored. Abstracting with credit is permitted. To copy otherwise, or republish, to post on servers or to redistribute to lists, requires prior specific permission and/or a fee. Request permissions from [permissions@acm.org](mailto:permissions@acm.org).

© 2023 Copyright held by the owner/author(s). Publication rights licensed to ACM.

1550-4859/2023/10-ART11 \$15.00

<https://doi.org/10.1145/3614431>

## 1 INTRODUCTION

**Wireless Power Transfer (WPT)** technology [20] has witnessed significant breakthroughs in recent years because of advantages of no-wiring, no-contact, and ease of maintenance. WPT allows energy to be delivered wirelessly from a transmitter to a receiver through electromagnetic waves. Exploiting the WPT technology helps construct the **Wireless Rechargeable Sensor Networks (WRSNs)** [18, 26, 28, 46]. For example, we can place wireless chargers at the appropriate locations in the WRSNs to provide continuous and stable power supply for the rechargeable sensors wirelessly. Owing to the fact that WRSNs greatly alleviate the energy limitation problem in **Wireless Sensor Networks (WSNs)** [30], they have been widely used in many fields, such as animal protection, healthcare, ecological environment detection, and so on [12, 29, 36, 44].

In practical charging scenarios, obstacles of arbitrary shapes and materials are ubiquitous. For example, in outdoor environments, where wildlife is monitored, trees, and stones are distributed. Similarly, in indoor environments, where temperature and humidity are monitored, there will inevitably be walls, glass, and furniture. According to the electromagnetic wave theory [4], electromagnetic waves can penetrate various obstacles (e.g., walls, trees, and glass) with different attenuation coefficients. Unfortunately, most traditional charger placement studies either ignore the existence of obstacles [7, 9, 10, 22, 50] or assume that electromagnetic waves cannot penetrate obstacles [21, 42, 47], which conflicts with the real environment. Recently, although a few work [23, 24] have considered the influences of obstacles on the propagation of electromagnetic waves, and established a charging model based on the Fresnel diffraction model to calculate the energy strength of the areas blocked by obstacles. However, this diffraction model is only suitable for metal obstacles. Besides, only when the sizes of the obstacles/apertures are comparable to the wavelength of wave, diffraction is observable. Nevertheless, in practical charging scenarios, obstacles of various materials have different penetration coefficients, and it is also impossible for all these obstacles to meet the above conditions in size. As a result, the applicability of existing methods is rather limited in practical scenarios.

To demonstrate the influences of the material, size, and location of obstacles on the propagation of electromagnetic waves, we conduct a testbed experiment by using the off-the-shelf TX91501 wireless charger produced by Powercast [34]. Figure 1 depicts the energy strength heatmap of the 2D plane with obstacles made of bricks and wood. It can be seen that these obstacles cannot completely block the propagation of electromagnetic waves, and the areas behind obstacles can still receive non-negligible energy. In the framework of electromagnetic wave theory [4], a major factor affecting the blocking effect of obstacles is the material of the obstacles. In particular, obstacles made of conducting materials, such as metal, will completely block the propagation of electromagnetic waves. However, when the electromagnetic waves encounter obstacles of insulator materials, they will penetrate these obstacles with different attenuation coefficients. As shown in Figure 1, the energy strength of the area blocked by the 5-cm-thick wooden board is significantly stronger than that of the area blocked by the wall with the same thickness. Another factor that affects the propagation of electromagnetic waves is the thickness of obstacles. From Figure 1, we can see the 10-cm-thick brick has a stronger blocking effect than the 5-cm-thick wall. This phenomenon shows that the thicker the obstacles, the stronger the blocking effect on electromagnetic waves. Hence, to achieve efficient wireless charging in real applications, it is essential to build a practical charging model with obstacles taking the material, size, and location of the obstacles into account, to obtain the eventually received energy by each sensor.

In this article, we focus on the problem of **Wireless chArger placement wIth obsTacles (WAIT)**. Formally, given a number of rechargeable sensors with fixed positions distributed on a 2D plane where obstacles of arbitrary shapes and materials exist, the WAIT problem is to place a

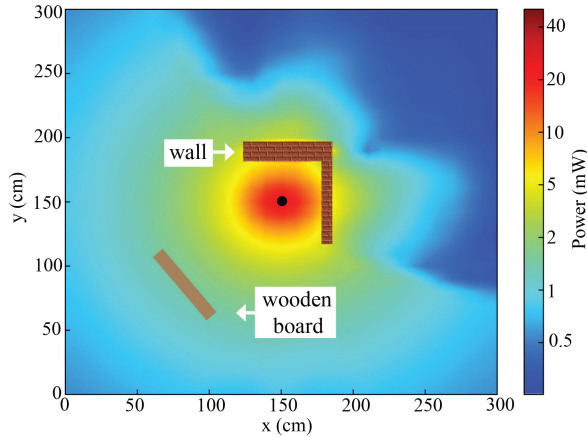


Fig. 1. A testbed experiment to explore the energy strength distribution when there are obstacles on the plane. An omnidirectional wireless charger is located at the center of the plane. Obstacles made of bricks and wood are distributed around the charger. The thickness of the vertical and horizontal walls are 5 cm and 10 cm, respectively. The thickness of the wooden board is 5 cm. We divided the whole experimental area into  $10 \text{ cm} \times 10 \text{ cm}$  grids and placed the sensor in each grid in turn to record the received energy strength.

limited number of omnidirectional wireless chargers on the plane, i.e., to determine their positions, such that the overall charging utility of all the sensors is maximized. Generally, we face several inherent challenges in solving the WAIT problem.

The first challenge is to build a practical charging model with obstacles. To choose appropriate positions for chargers, we need to know how much energy each sensor can be obtained no matter where the chargers are placed. Since the material, size, and location of obstacles all have significant impacts on the propagation of electromagnetic waves, it requires us to model the charging environment with obstacles by jointly considering these parameters, to obtain the electromagnetic wave intensity of the areas blocked by obstacles.

The second challenge is that the WAIT problem is nonlinear and continuous. WAIT is nonlinear, because the received power is nonlinear with charging distance, which makes our objective (i.e., charging utility) nonlinear. WAIT is continuous, because the positions available for charger placement are continuous values, which implies there are an infinite number of candidate placement positions.

To address these challenges, we introduce shadow fading [4] to formalize the influences of obstacles on electromagnetic wave propagation, and further combine the Friis's free space model to build our practical charging model with obstacles. We carry out extensive testbed experiments to verify the correctness of this model. For the second challenge, to tackle the problem of charging power is nonlinear with distance, we design a piecewise constant function to approximate the nonlinear charging power with bounded energy error  $\epsilon$  guarantee, and further divide the whole area into multiple subareas. In order to tackle the problem of continuous search place, we develop a Dominating Coverage Set extraction algorithm to reduce the continuous solution space to a limited number.

In summary, the main contributions of this work are summarized as below.

- To the best of our knowledge, this is the first work to study the physical characteristics of electromagnetic waves that can penetrate obstacles of various materials. We jointly consider

Table 1. Notations

Symbol	Meaning
$s_i$	Sensor $i$ , or its location
$c_i$	Wireless charger $i$ , or its location
$o_h$	Obstacle $h$ on the plane
$N$	Number of sensors
$M$	Number of wireless chargers
$H$	Number of obstacles on the plane
$P_r(\cdot)$	Charging power function
$U(\cdot)$	Utility function
$D$	Farthest charging distance of the charger
$P_{th}$	Threshold for charging utility function

the material, size and location of obstacles, and build a practical charging model to obtain the energy strength of the areas blocked by obstacles. And then, we aim to select suitable placement locations for a limited number of chargers based on the proposed charging model to maximize the overall charging utility.

- We formulate the charging utility maximization problem with obstacles as a WAIT problem, and prove the NP-hardness of WAIT. To reduce the computational complexity, we discretize the space to solve the problem of infinite candidate locations on a 2D continuous plane. We propose the so-called Dominating Coverage Set extraction algorithm to select the candidate points with the largest number of covers on the plane. Then, we design a greedy algorithm with an approximation ratio of  $1 - 1/e - \varepsilon$  to solve the WAIT problem.
- We conduct extensive simulations and testbed experiments to verify the performance of the proposed scheme. The experimental results show that our WAIT scheme achieves excellent charging performance and significantly outperforms comparison algorithms.

The rest of this article is organized as follows. Section 2 introduces preliminaries, including the simplified charging model, charging utility model and the problem formulation. Section 3 presents the practical charger placement scheme. Sections 4 and 5 show the results of simulations and field experiments, respectively. Section 6 discusses related issues. Section 7 reviews the related work and Section 8 concludes this article.

## 2 PRELIMINARIES

### 2.1 Network Model

We suppose that there is a set of omnidirectional wireless rechargeable sensors  $S = \{s_1, s_2, \dots, s_N\}$  placed on a 2D plane  $\Omega$  with fixed positions, where  $N$  is the number of sensors. We also have  $M$  omnidirectional wireless chargers, denoted as  $C = \{c_1, c_2, \dots, c_M\}$ , which can be placed anywhere on the 2D plane. If no confusion is caused, then we still use  $s_i$  and  $c_j$  to represent the location of rechargeable sensor  $s_i$  and wireless charger  $c_j$ , respectively.

Meanwhile, there are  $H$  static obstacles  $O = \{o_1, o_2, \dots, o_H\}$  with arbitrary shapes and materials distributed on the two-dimensional plane. Here, any sensors and chargers cannot be placed inside obstacles. We also use  $o_h$  to denote the location of obstacle  $o_h$ . To simplify the model, we assume that all obstacles are made of uniform and single material. The material and location of each obstacle on the plane can be identified beforehand by using localization and sensing techniques proposed in References [13, 31, 38, 39]. For a quick reference, the major notations are summarized in Table 1.

## 2.2 Simplified Charging Model

To simplify the analysis, we first ignore the influences of obstacles that exist on the plane and use Friis's free space equation [26] as the energy transmission model. This model is widely used in existing studies [7, 9, 10, 19, 30, 42, 45, 50]. In this model, the energy received by a sensor is determined by the source power of the charger and the distance between the charger and the sensor. According to the profiling experiments in Reference [17], the correctness and effectiveness of this model have been proven. Assume that a wireless charger is located at  $c_j$  and a sensor is located at  $s_i$ , the power  $p(s_i, c_j)$  received by the sensor can be quantified as

$$p(s_i, c_j) = \frac{\alpha}{(d(s_i, c_j) + \beta)^2} \cdot P_T, \quad (1)$$

where  $\alpha$  and  $\beta$  are known constants determined by the intrinsic hardware of the device and the surrounding environment.  $d(s_i, c_j)$  is the Euclidean distance between charger  $c_j$  and sensor  $s_i$ .  $P_T$  is the source power.

Note that the influences of ubiquitous obstacles in the network are not considered in Friis's space equation. As shown in Figure 1, obstacles with different materials and sizes have different effects on the propagation of electromagnetic waves. Obviously, using Equation (1) alone cannot obtain the energy actually received by the sensors blocked by obstacles. Therefore, how to jointly consider the influences of the material, size, and location of obstacles on the charging process, and build a practical charging model with obstacles is a critical issue to achieve efficient charger placement in real scenario. With this consideration, we will describe the design details of our practical charging model with obstacles in Section 3.1.

## 2.3 Charging Utility Model

Because of hardware constraints or practical demand, the power received by rechargeable sensors usually has an upper bound  $P_{th}$ . Formally, the harvested power by a sensor must not exceed the threshold  $P_{th}$  regardless of the charging power of chargers. Therefore, we propose the *charging utility* model as follows:

$$U_i(x) = \begin{cases} \frac{1}{P_{th}} \cdot x, & x \leq P_{th}, \\ 1, & x > P_{th}, \end{cases} \quad (2)$$

where  $U_i(x)$  is the charging utility of the sensor  $s_i$ , and  $x$  represents the power received by it. In this model, when the charging power is less than or equal to the preset threshold  $P_{th}$ , the charging utility is proportional to the power received by the sensor. When the charging power exceeds  $P_{th}$ , the charging utility becomes constant.

## 2.4 Problem Formulation

In this work, we study a fundamental problem of WAIT: how to place a fixed number of omnidirectional wireless chargers on a 2D plane  $\Omega$  with obstacles, such that the overall charging utility of all sensors is maximized. The definition of the WAIT problem is given as follows:

*Given a limited number of rechargeable sensors with fixed positions distributed on a 2D plane where obstacles exist, the objective is to find a charging placement scheme that the overall charging utility of all the sensors is maximized, under the constraint that sensors and chargers must be placed on the plane  $\Omega$  and cannot be placed inside the obstacles  $O$ . We define the overall charging utility as the sum of the charging utilities of all sensors. Formally, we define the WAIT problem as follows:*

$$\text{maximize} \quad \sum_{i=1}^N U_i \left( \sum_{j=1}^M p(s_i, c_j) \right), \quad (3)$$

subject to

$$\begin{aligned} s_i, c_j &\in \Omega, \\ s_i, c_j &\notin O. \end{aligned} \tag{4}$$

The following theorem shows the hardness of our WAIT problem.

**THEOREM 2.1.** *The WAIT problem is NP-complete.*

**PROOF.** We consider a special case of WAIT, named WAIT-S, by removing obstacles. We show that the decision version of WAIT-S is NP-hard, so is WAIT.

Note that since there are no obstacles on the plane, each charger has a disk-shaped charging area with a constant radius of  $D$ , where  $D$  is the farthest charging distance. We assume that the charging utility of each sensor is 1, as long as it is covered by a charger. Thus, each sensor can be regarded as a point, and the WAIT-S problem changes to the problem of covering as many points as possible by  $M$  disks with uniform radius  $D$ . Thus, we can see that the WAIT-S is exactly the partial disk covering problem [43]. The theorem thus follows.  $\square$

### 3 PROPOSED SCHEME

In this section, we propose our practical charger placement scheme for the WAIT problem. We first comprehensively consider the influences of the material, size, and location of the obstacles on the charging process, and build our practical charging model with obstacles by introducing shadow fading. We also conduct testbed experiments to verify the correctness of this model. Then, we approximate the charging power, which is a continuous function of distance, into a piecewise constant function. By this means, the charging area of each charger is divided into multiple subareas. Next, we develop a Dominating Coverage Set extraction algorithm to reduce the continuous search space on a 2D plane to a finite number without performance loss. Finally, we reformulate the WAIT problem as maximizing a monotone submodular optimization problem, and design a greedy algorithm to address this problem with  $1 - 1/e - \varepsilon$  approximation ratio.

#### 3.1 Practical Charging Model with Obstacles

In this subsection, we aim to build a practical charging model with obstacles, so that we can calculate the energy received by the sensors blocked by obstacles. At first, we analyze the influences of obstacles on the propagation of electromagnetic waves. According to the wireless communication theory [1], when electromagnetic wave encounters obstacles in the process of propagation, it will change randomly, resulting in the random change in the received power of the sensor at a given location. Thus, the material, size, and location of the obstacles will lead to random attenuation of electromagnetic waves, only statistical models can be used to characterize this random attenuation.

Therefore, we introduce *shadow fading* to characterize the random attenuation of electromagnetic waves. Shadow fading, also known as slow fading, is a phenomenon in which the received signal strength decreases due to the shadowing effect caused by obstacles. It will attenuate the signal power, and even block the signal in severe cases [1]. The log-normal shadowing model has been confirmed by measured data to accurately model the variation of received power in indoor and outdoor electromagnetic wave propagation environments [11, 33].

The log-normal shading model takes the ratio of transmitted and received power  $\psi = P_t/P_r$  ( $P_t$  and  $P_r$  represent transmit power and receive power, respectively) as a lognormally distributed random variable. Thus, we have the following energy loss expressed as

$$P_{loss} = P(\psi) = \frac{\zeta}{\sqrt{2\pi}\sigma_{\psi_{dB}}\psi} \exp\left[-\frac{(10\lg\psi - \mu_{\psi_{dB}})^2}{2\sigma_{\psi_{dB}}^2}\right], \tag{5}$$

where  $\zeta = 10/\ln 10$ ,  $\mu_{\psi_{dB}}$  is the mean of  $\psi_{dB} = 10 \lg \psi$  in dB, and  $\sigma_{\psi_{dB}}$  is the standard deviation of  $\psi_{dB}$  in dB. A large number of outdoor channel measurements show that the standard deviation  $\sigma_{\psi_{dB}}$  ranges from 4 to 13 dB [3, 15]. The mean power  $\mu_{\psi_{dB}}$  depends on path loss and obstacles properties in the area.  $\mu_{\psi_{dB}}$  varies with distance. One reason is that the deterministic loss changes with distance, and the other reason is the increase of charging distance may give a rise to the number of obstacles, resulting in an increase in the average attenuation.

When shadow fading is dominated by blocking attenuation, the Gaussian model of average received power can be analyzed with the following fading model. The attenuation of the electromagnetic wave traveling through an obstacle of length  $l$  can be approximately equal to [1]

$$P_{loss} \approx e^{-\frac{1}{l} \cdot (1-\eta)}, \quad (6)$$

where  $\eta$  is an attenuation coefficient constant independent of obstacle size, and also is unique for each material [13, 39]. Here,  $\eta = 1$  means that electromagnetic waves cannot penetrate obstacles. On the contrary, the smaller the  $\eta$  is, the electromagnetic waves can penetrate obstacle with less loss.

Note that, the traveling distance of electromagnetic wave in obstacle is related to the relative position of charger, sensor, and obstacle. If one of them changes, then  $l$  it will also vary. To help understand, we use Figure 2 to further illustrate this situation. It can be seen that an obstacle is located on the **Line-of-Sight (LOS)** of sensor  $s$  and charger  $c$ , which hinders the propagation of the electromagnetic wave. Although the shape of the obstacle is irregular, we only need to simply draw a line from the charger to the sensor, the traveling distance  $l$  of the wave in the obstacle can be obtained.

In practical charging scenarios, when there are multiple obstacles between the charger and sensor, the attenuation of the electromagnetic wave is a superposition of the shadow fading effects caused by the multiple obstacles:

$$P_{loss} = e^{-\frac{1}{l_1} \cdot (1-\eta_1)} \times e^{-\frac{1}{l_2} \cdot (1-\eta_2)} \times \cdots \times e^{-\frac{1}{l_H} \cdot (1-\eta_H)} = e^{-\sum_{h=1}^H \frac{1}{l_h} \cdot (1-\eta_h)}. \quad (7)$$

To sum up, we combine the Friis's space equation and the shadow fading model to build our practical charging model with obstacles:

$$P_r(s_i, c_j) = \frac{\alpha \cdot P_T}{(d(s_i, c_j) + \beta)^2} \cdot (1 - P_{loss}) = \frac{\alpha \cdot P_T}{(d(s_i, c_j) + \beta)^2} \cdot (1 - e^{-\sum_{h=1}^H \frac{1}{l_h} \cdot (1-\eta_h)}). \quad (8)$$

Thus, we have

$$P_r(s_i, c_j) = \begin{cases} \frac{\alpha \cdot P_T}{(d(s_i, c_j) + \beta)^2}, & s_i c_j \cap o_h = \emptyset, \\ \frac{\alpha \cdot P_T}{(d(c, s) + \beta)^2} \cdot (1 - e^{-\sum_{h=1}^H \frac{1}{l_h} \cdot (1-\eta_h)}), & s_i c_j \cap o_h \neq \emptyset, \end{cases} \quad (9)$$

where the condition  $s_i c_j \cap o_h = \emptyset$  represents the line connecting sensor  $s_i$  and charger  $c_j$  should not cross any obstacle, and vice versa.

We assume the power received by one sensor from multiple chargers is additive [6, 8, 17, 41, 48, 49]. That is, given a sensor placement location, the total power  $P(s_i)$  received by sensor  $s_i$  is

$$P(s_i) = \sum_{j=1}^M P(s_i, c_j). \quad (10)$$

We conduct test-bed experiments to verify the charging model with obstacles. We use an off-the-shelf TX91501 as a wireless charger and a sensor equipped with P2110 as a wireless rechargeable sensor, both of them are produced by Powercast [34]. We fix the charger's position, and vary the

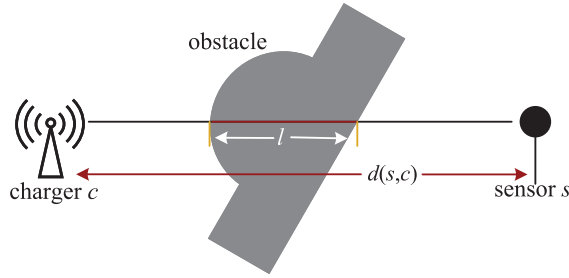


Fig. 2. Schematic of charging with obstacle.

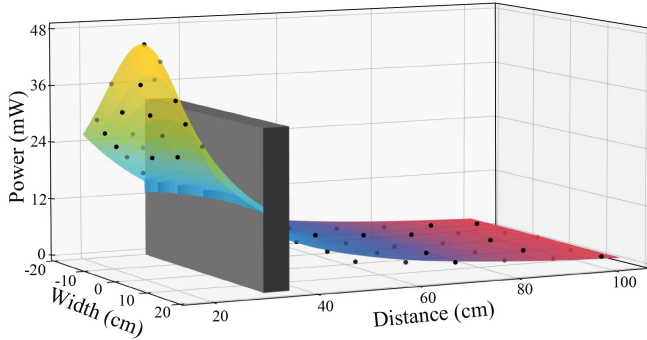


Fig. 3. Comparison of measured data (black dots) and simulated fitting data (mesh). The black cuboid represents an obstacle with a thickness of 5 cm. Fitted results are based on  $\alpha = 8.2$ ,  $\beta = 2.8$  and  $\eta_{brick} = -1.8$ .

distance between the charger and the sensor from 20 to 100 cm. Note that we place the 5-cm-thick obstacle 35 cm away from the charger, and measure the energy received by the sensor behind the obstacle. To evaluate the correctness of our charging model, we also use Equation (9) to fit the experimental data. As shown in Figure 3, the fitting results illustrate that our practical charging model is suitable for real charging scenarios with obstacles.

Next, we use bricks and paper as obstacles, and verify the correctness of our charging model by setting the value of thicknesses to 10 cm and 15 cm, respectively. As shown in Figure 4, the charger and the sensor are placed on both sides of the obstacle. We also fix the position of the charger, and record the received energy by changing the distances between the sensor and the charger from 50 to 100 cm. From Figure 5, we can see that the measured data fit well with the simulation results, which further demonstrates the correctness of our proposed charging model with obstacles.

### 3.2 Charging Power Approximation and Area Discretization

After the positions and the materials of obstacles are obtained by using localization and sensing technology [13, 31, 38, 39], the power attenuation coefficient  $1 - e^{-\sum_{h=1}^H \frac{1}{l_h} \cdot (1 - \eta_h)}$  caused by obstacles in Equation (8) can be regarded as a constant. Let  $\mu$  denote the product of the power attenuation coefficient and the source power, the energy  $P_r(d)$  received by the sensor from the charger with distance  $d$  can be calculated as follows:

$$P_r(d) = \frac{\mu \cdot \alpha}{(d + \beta)^2}. \quad (11)$$

Note that,  $\mu = 1$  means that there do not exist obstacles between the charger and the sensor.

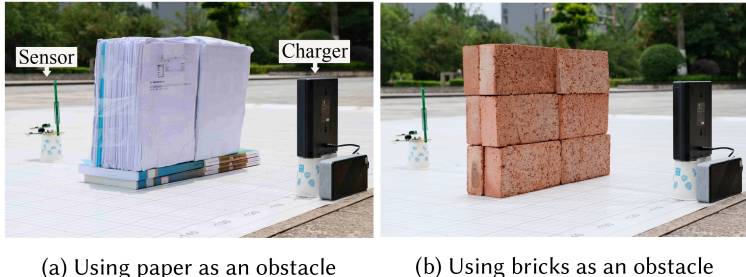


Fig. 4. Testbed experiments to explore the relationship between material, thickness of obstacles, and energy strength.

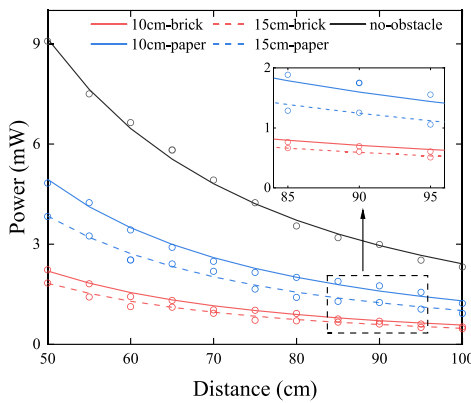


Fig. 5. A testbed experiment to measure the change of energy strength from 50 to 100 cm in charging distance when obstacles of different materials (i.e., paper and brick) and thicknesses (i.e., 10 cm and 15 cm) are placed between the sensor and the charger. We set  $\alpha = 8.2$ ,  $\beta = 2.8$ ,  $\eta_{brick} = -1.8$ ,  $\eta_{paper} = -6.7$ . The dots in the figure represent the measured data.

Since the charging power is nonlinear with the distance, we introduce a piecewise constant function to approximate the charging power  $P_r(d)$  to  $\tilde{P}_r(d)$ . The definition of  $\tilde{P}_r(d)$  is given as follows:

$$\tilde{P}_r(d) = \begin{cases} P_r(l(1)), & d = l(0), \\ P_r(l(k)), & l(k-1) < d \leq l(k) \ (k = 1, 2, \dots, K), \\ 0, & d > l(K), \end{cases} \quad (12)$$

where  $l(0) = 0$ ,  $l(K) = D$ . Moreover,  $K$  refers to the total number of constant segments of the piecewise function. Obviously,  $K$  is a key parameter that controls the approximation error. With a smaller  $K$ , lower computational complexity will be introduced, but the approximation error tends to be larger, and vice versa.

We have the following theorem to ensure that the approximation error is less than  $\varepsilon$ . Note that  $\varepsilon$  is a predetermined error threshold.

**THEOREM 3.1.** *We set  $l(0), l(K) = D$ , and  $l(k) = \beta((1 + \varepsilon)^{\frac{k}{2}} - 1)$ , ( $k = 1, 2, \dots, K - 1$ ). Then, we get  $K = \lceil \frac{\ln(P_r(0)/P_r(D))}{\ln(1+\varepsilon)} \rceil = 2\lceil \frac{\ln(1+\frac{D}{\beta})}{\ln(1+\varepsilon)} \rceil$ , the approximation error is subject to*

$$1 \leq \frac{\tilde{P}_r(d)}{P_r(d)} \leq 1 + \varepsilon, \quad (d \leq D). \quad (13)$$

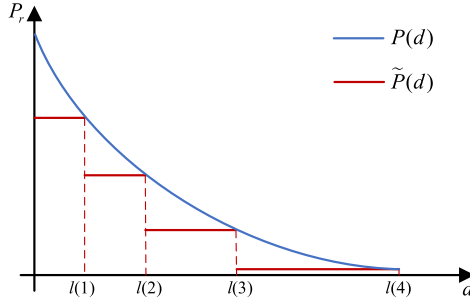


Fig. 6. Power approximation.

For ease of understanding, we use Figure 6 as an example to illustrate this charging power approximation. In Figure 6,  $K$  is set to 4, and the blue curve is the energy actually received by the sensor from the charger, and the red segments are the approximate energy after power discretization using Equation (12).

Due to geometric symmetry, the placeable area for the charger to transfer energy to sensor  $s_i$  can also be discretized into  $K$  concentric rings centered at  $s_i$ . When the charger is located at different locations within a certain ring, the energy received by the sensor covered by the charger can be approximately regarded as equal. Note that, because of the influences of obstacles, the shapes of concentric rings of each sensor may be irregular. Figure 7 shows an example for which we draw three concentric rings for three sensors with radius  $l(1)$ ,  $l(2)$ ,  $l(3)$ , and obtain 22 subareas. We can see that the shapes of the three concentric rings of sensor  $s_1$  become irregular because of the obstacle. In addition, the charger placement areas for  $s_1$ ,  $s_2$ , and  $s_3$  have an overlapping region, which is divided into several subareas (i.e.,  $a_9$  and  $a_{10}$ ) by concentric rings. It is worth noting that  $s_1$ ,  $s_2$ , and  $s_3$  can receive energy from the charger simultaneously when the charger is placed in these overlapping areas.

Next, We have the following theorems for area discretization:

**THEOREM 3.2.** *Let  $\tilde{P}_r(s_i)$  be the approximated charging power received by sensor  $s_i$  in each subarea, if  $P(s_i) = 0$ , then  $\tilde{P}(s_i) = 0$ ; otherwise, the approximate error is*

$$1 \leq \frac{P_r(s_i)}{\tilde{P}_r(s_i)} \leq 1 + \varepsilon. \quad (14)$$

**PROOF.** We omit the proof due to space limitation.  $\square$

**THEOREM 3.3.** *The number of subareas after area discretization is  $O(N^2\varepsilon^{-2}H^2)$ .*

**PROOF.** According to Theorem 3.1, each sensor has a placeable area that is divided into  $K = O(\varepsilon^{-1})$  concentric rings. Moreover, there are  $N$  sensors on the plane, which generates  $O(N\varepsilon^{-1})$  subareas in total. Further, consider that there are  $H$  obstacles, the total number of overlapping areas due to the obstacles is  $O(N\varepsilon^{-1} + H)$ . Therefore, the number of divided subareas is squared, i.e.,  $O((N\varepsilon^{-1} + H)^2)$ , which can be simplified to  $O(N^2\varepsilon^{-2}H^2)$ .  $\square$

### 3.3 Dominating Coverage Set Extraction

After area discretization, the whole 2D plane is divided into multiple subareas. Then, in this subsection, we develop a **Dominating Coverage Set (DCS)** extraction algorithm to extract candidate placement subareas for chargers from those divided subareas.

Then, we give the following definitions.

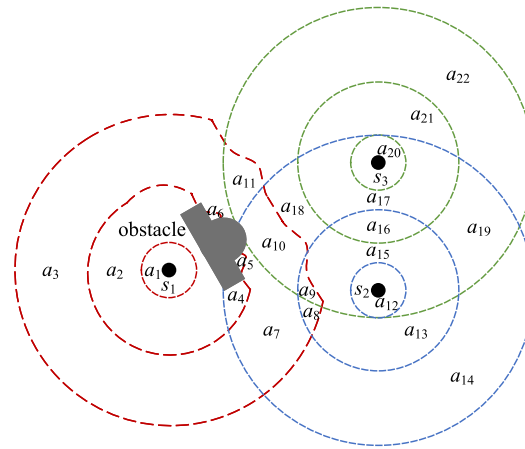


Fig. 7. Illustration of area discretization.

**Definition 3.4 (Dominance).** Given the placement locations of two chargers  $c_1, c_2$ , and their corresponding sensor coverage sets  $S_1$  and  $S_2$ . If  $S_1 = S_2$ , then we say  $c_1$  is equivalent to  $c_2$ ; if  $S_2 \subset S_1$ , then we define  $c_1$  dominates  $c_2$ .

**Definition 3.5 (Dominating Coverage Set).** Given a set of sensors  $S_i$  covered by a charger  $c_i$ , if there does not exist a sensor coverage set  $S_j$  with charger's placement location  $c_j$  such that  $S_i \subset S_j$ , then we say  $S_i$  is a DCS.

**Definition 3.6 (Candidate Covered Set of Sensors).** The sensors in the Candidate Covered Set of Sensors  $\hat{S}$  of subarea  $a_i$  are those sensors that can be charged by chargers located in  $a_i$  with non-zero power.

Since it is always better to choose DCSs than a subset of them, we focused on finding all possible DCSs and their corresponding placement locations.

For better comprehension, we use Figure 7 to illustrate the process of extracting DCSs. As shown in Figure 7, the charger placeable areas of  $s_1, s_2$ , and  $s_3$  are discretized into multiple subareas. In Figure 7, the Dominating Coverage Sets are  $a_9$  and  $a_{10}$ , since when a charger is placed in these subareas, their candidate covered set of sensors are all  $\{s_1, s_2, s_3\}$ . The detailed process of Dominating Coverage Set extraction algorithm is given in Algorithm 1.

After getting all the DCSs and corresponding subareas, we need to choose  $M$  DCSs to place the all chargers to maximize the overall charging utility. The specific method will be described in detail in the next subsection.

### 3.4 Problem Reformulation and Solution

In this subsection, we detail how to select a given number of locations to place chargers to maximize the overall charging utility. Particularly, we first reformulate the WAIT problem and prove that it is a submodular function. Consequently, we propose a greedy algorithm to solve the problem.

We use  $\Pi$  to denote the set of all DCS solutions obtained after executing Algorithm 1. For each DCS in  $\Pi$ , we can calculate the charging power and charging utility received by each sensor when the charger is located at the corresponding placement location. Then, we rewrite the WAIT problem as follows:

**ALGORITHM 1:** Dominating Coverage Set Extraction Algorithm

**Input:** The set of sensors  $S$ , the farthest charging distance  $D$ , the approximation error threshold  $\varepsilon$ , the constant  $\beta$ , the obstacles on the plane.

**Output:** All DCSs and their corresponding subareas.

- 1: Calculate the number of segments  $K$  for the piecewise constant function:  $K = 2\lceil \frac{\ln(1+\frac{D}{\beta})}{\ln(1+\varepsilon)} \rceil$ ;
- 2:  $A \leftarrow \emptyset$ ;
- 3: **for** each sensor  $s_i \in S$  **do**
- 4:     Draw the  $K$  discretized charger placeable area of  $s_i$  using Equation (12).
- 5: **end for**
- 6: Add all discretized subareas to  $A$ ;
- 7: **for** each subarea  $a_i \in A$  **do**
- 8:     Calculate the corresponding candidate covered set of sensors for each subarea  $a_i$ ;
- 9:     Add the candidate covered set of sensors and subarea  $a_i$  into the candidate DCSs;
- 10: **end for**
- 11: Identify and remove all the DCSs that are subsets of other DCSs in candidate DCSs;
- 12: Return DCSs and their corresponding subareas;

Let  $b_j$  denote a binary variable, which can be used to indicate whether the  $j$ th placement location in  $\Pi$  is selected or not. Therefore, the **Problem 1** in Section 2.4 can be reformulated as

$$\text{maximize} \quad \sum_{i=1}^N U_i \left( \sum_{c_j \in \Pi} b_j \tilde{P}(s_i, c_j) \right), \quad (15)$$

subject to

$$\sum_{j=1}^{|\Pi|} b_j = M \quad b_j \in \{0, 1\}. \quad (16)$$

In the following, we prove that the objective function  $U(x)$  has three properties: nonnegativity, monotonicity and submodularity. Therefore, we propose a  $(1 - \frac{1}{e} - \varepsilon)$  approximation algorithm to solve **Problem 2** as shown in Algorithm 2. We first give the following definition.

**Definition 3.7 (Nonnegativity, Monotonicity, and Submodularity).** Given a non-empty finite set  $S$ , and a function  $f$  defined on the power set  $2^S$  of  $S$  with real values.  $f$  is called nonnegative, monotone, and submodular if and only if it satisfies the following conditions, respectively:

1.  $f(\emptyset) = 0$  and  $f(X) \geq 0$  for any  $X \subseteq S$  (nonnegative);
2.  $f(X) \leq f(Y)$  for all  $X \subseteq Y \subseteq S$  or equivalently:  $f(X \cup \{e\}) - f(X) \geq 0$  for any  $X \subseteq S$  and  $e \in S \setminus X$  (monotone);
3.  $f(X \cup \{e\}) - f(X) \geq f(Y \cup \{e\}) - f(Y)$  for any  $X \subseteq Y \subseteq S$  and  $e \in S \setminus Y$  (submodular).

Then, we have the following theorem.

**THEOREM 3.8.** *The objective function  $U(x)$  is nonnegative, monotone, and submodular.*

**PROOF.** To check whether the  $U(X)$  in Equation (15) is a submodular function, we need to verify whether  $U(X)$  satisfies the three conditions in Definition 4. Then, we prove that  $U(X)$  satisfies nonnegative, monotone, and submodularity properties, respectively.

1. Obviously, the charging utility function  $U(X) = 0$  when  $X = \emptyset$ , since there is no charger on the plane to provide charging service for sensors. And we can know that  $U(X)$  is a

**ALGORITHM 2:** Greedy Algorithm for Placing Chargers

**Input:** The number of chargers  $M$ , all candidate DCSs  $\Pi$  and their corresponding locations, charging utility function  $U(X)$ .

**Output:** The final placement location set for chargers  $C$  and overall charging utility  $U(C)$ .

```

1:  $C \leftarrow \emptyset;$ 
2: while  $C \leftarrow \emptyset$  do
3:    $c^* \leftarrow \arg \max_{c \in \Pi \setminus C} (U(C \cup \{c\}) - U(C));$ 
4:    $C \leftarrow C \cup \{c^*\};$ 
5: end while
```

6: Randomly select a point as a placement location for charger in each subarea;

7: Return  $C, U(C)$ ;

nonnegative function from Equation (2), that is, any charger can provide nonnegative charging power to the sensor. Therefore, the  $U(X)$  function satisfies nonnegativity.

2. It is also clear that when a new candidate placement location is selected, the charging utility will increase, because  $U(X)$  defined in Equation (2) is non-decreasing. Formally, for all  $X \subseteq Y \subseteq S$ , we have

$$U(X) = \sum_{i=1}^N U_X(s_i) \leq \sum_{i=1}^N U_Y(s_i) = U(Y). \quad (17)$$

Therefore, the  $U(X)$  function satisfies monotonicity.

3. For all  $X \subseteq Y \subseteq S$ , we need to prove that  $f(X \cup \{e\}) - f(X) \geq f(Y \cup \{e\}) - f(Y)$ . First, we define a function  $h(A, i) = \sum_{c_j \in A} \tilde{P}_r(s_i, c_j)$ . The observation is that  $h(\cdot, i)$  is an increasing function, since more chargers provide more charging power. Then, for the candidate placement locations sets  $X \subseteq Y \subseteq \Pi$  and a candidate placement location  $e \in \Pi \setminus Y$ , we can obtain that  $h(X, i) \leq h(X \cup \{e\}, i), h(Y, i) \leq h(Y \cup \{e\}, i)$ . Therefore, we have

$$[U_i(h(X \cup \{e\}, i) - U_i(h(X, i))] - [U_i(h(Y \cup \{e\}, i) - U_i(h(Y, i))] \geq 0, \quad (18)$$

because for any  $0 \leq y_1 \leq y_2$  and  $\Delta y \geq 0$ ,

$$[U_i(y_1 + \Delta y) - U_i(y_1)] - [U_i(y_2 + \Delta y) - U_i(y_2)] \geq 0 \quad (19)$$

and

$$h(X \cup \{e\}, i) - h(X, i) = h(Y \cup \{e\}, i) - h(Y, i) = h(\{e\}, i). \quad (20)$$

Thus, we have

$$\begin{aligned} & [f(X \cup \{e\}) - f(X)] - [f(Y \cup \{e\}) - f(Y)] \\ &= \{[U_i(h(X \cup \{e\}, i) - U_i(h(X, i))] - [U_i(h(Y \cup \{e\}, i) - U_i(h(Y, i))]\} \geq 0. \end{aligned} \quad (21)$$

Finally, we obtain  $f(X \cup \{e\}) - f(X) \geq f(Y \cup \{e\}) - f(Y)$  and prove that the  $U(X)$  function satisfies submodularity.  $\square$

Next, we design a greedy algorithm to select the placement locations for chargers. Algorithm 2 is essentially a greedy algorithm, in each iteration, we add the location that maximizes the marginal utility of the objective function into  $C$ , i.e.,  $c^* \leftarrow \arg \max_{c \in \Pi \setminus C} (U(C \cup \{c\}) - U(C))$ . Then, we randomly choose a placement location for the charger in each subarea, since when a charger is placed at any point in the subarea, the power it transmits to the surrounding sensors is approximately constant. The detailed process of Greedy-based Placement Algorithm for Chargers is given in Algorithm2.

**THEOREM 3.9.** *Our algorithm achieves an approximate ratio of  $1 - \frac{1}{e} - \varepsilon$ .*

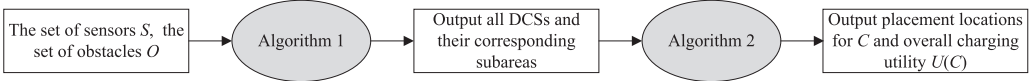


Fig. 8. Relations between algorithms.

**PROOF.** According to the results in Reference [14], a greedy algorithm is used to maximize a submodular function and achieves  $1 - \frac{1}{e}$  approximation ratio. Therefore, the approximate ratio of our Algorithm2 is also  $1 - \frac{1}{e}$ . Let  $\Pi^*$  denote the optimal solution to the problem P2, then we have

$$\sum_{i=1}^N U_i \left( \sum_{c_j \in \Pi} b_j \tilde{P}(s_i, c_j) \right) \geq \left(1 - \frac{1}{e}\right) \sum_{i=1}^N U_i \left( \sum_{c_j \in \Pi^*} b_j \tilde{P}(s_i, c_j) \right). \quad (22)$$

By Theorem 3.1, we can obtain  $\tilde{P}_r(s_i, c_j) \geq \frac{1}{1+\varepsilon} P_r(s_i, c_j)$ . Then, by the property of the charging utility function, we have

$$\sum_{i=1}^N U_i \left( \sum_{c_j \in \Pi^*} b_j \tilde{P}(s_i, c_j) \right) \geq \sum_{i=1}^N U_i \left( \sum_{c_j \in \Pi^*} \frac{1}{1+\varepsilon} b_j P(s_i, c_j) \right) \geq \frac{1}{1+\varepsilon} \cdot \sum_{i=1}^N U_i \left( \sum_{c_j \in \Pi^*} b_j P(s_i, c_j) \right). \quad (23)$$

Combining inequality Equations (22) and (23), we have

$$\begin{aligned} \sum_{i=1}^N U_i \left( \sum_{c_j \in \Pi} b_j \tilde{P}(s_i, c_j) \right) &\geq \left(1 - \frac{1}{e}\right) \cdot \frac{1}{1+\varepsilon} \cdot \sum_{i=1}^N U_i \left( \sum_{c_j \in \Pi^*} b_j P(s_i, c_j) \right) \\ &\geq \left(1 - \frac{1}{e} - \varepsilon\right) \cdot \sum_{i=1}^N U_i \left( \sum_{c_j \in \Pi^*} b_j P(s_i, c_j) \right). \end{aligned} \quad (24)$$

Hence, the approximate ratio of the WAIT algorithm is  $1 - \frac{1}{e} - \varepsilon$ .  $\square$

**THEOREM 3.10.** *The time complexity of the WAIT algorithm is  $O(MN^4\varepsilon^{-4}H^4)$ .*

**PROOF.** First, the algorithm needs to discretize the charger placement area of all sensors according to obstacles on the plane and error threshold  $\varepsilon$ . The time complexity of this step is thus  $O(N^2\varepsilon^{-2}H^2)$  according to Theorem 3.3. Then, we need to enumerate each subarea to select the Dominating Coverage Sets, which time complexity is  $O(N^4\varepsilon^{-4}H^4)$ . Finally, in the greedy algorithm, the loop will be done  $M$  times, so the final result of time complexity is  $O(MN^4\varepsilon^{-4}H^4)$ .  $\square$

### 3.5 Relations of Algorithms

We draw a paradigm (see Figure 8) to illustrate the relationships between our proposed algorithms for making our solution more clear.

First, Algorithm 1 is called with the set of sensors  $S$  and the set of obstacles  $O$  as parameters. Then, Algorithm 1 is applied to generate all Dominating Coverage Sets and their corresponding subareas. Finally, Algorithm 2 is executed to obtain the final placement location set for chargers  $C$  and overall charging utility  $U(C)$ .

## 4 SIMULATIONS

In this section, to demonstrate our scheme is suitable for practical scenario with obstacles, simulations are conducted by comparing it with three other algorithms in terms of the number of chargers  $M$ , number of sensors  $N$ , error threshold  $\varepsilon$ , and power threshold  $P_{th}$ .

Table 2. Simulation Parameters

Parameters	Values
Network area	20 m × 20 m
Number of sensors	18
Number of chargers	12
Source power $P_T$ (W)	3
Farthest charging distance for chargers (m)	3
Threshold for charging utility function (mW)	1
Approximation error $\epsilon$	0.2
Attenuation coefficient of wood $\eta_{wood}$	-38.1
Attenuation coefficient of brick $\eta_{brick}$	-1.8
Attenuation coefficient of metal $\eta_{metal}$	1

#### 4.1 Simulation Setup

We consider a WRSN consisting of 18 sensors equipped with an omnidirectional antenna, which are placed within a 20 m × 20 m square area. We also have 12 omnidirectional chargers with working power of 3 W [35, 40, 42]. There are five obstacles in the square, and their materials are metal, wood, and brick, respectively. Among these materials, metal can completely block the transmitting power, the brick will bring serious electromagnetic wave attenuation, while the impact of wood is significantly weaker. The parameters of the practical charging model with obstacles in Equation (9) are set as  $\alpha = 8.2$ ,  $\beta = 2.8$ ,  $\eta_{wood} = -38.1$ ,  $\eta_{brick} = -1.8$ ,  $\eta_{metal} = 1$ . All these parameters are verified by filed experiments (see Figures 1, 3, and 5). The default simulation parameters are shown in Table 2. Moreover, all sensors and chargers cannot be placed inside obstacles.

To evaluate the performance of the proposed WAIT scheme, we compare it with the following three charging placement algorithms.

**Heterogeneous wIreless charger Placement with Obstacles (HIPO)** algorithm [42] is an algorithm for placing directional chargers on a 2D plane where obstacles exist. HIPO assumes that all obstacles would completely block the propagation of the electromagnetic waves, resulting in multiple “holes” where the sensors cannot receive any energy from the charger. After building a charging model with obstacles, HIPO maximizes the overall charging utility through a greedy-based charger placing method. For fair comparisons, in our simulations, the chargers placed by HIPO are omnidirectional.

**Wireless Charger Placement (WCP)** algorithm is an algorithm for placing omnidirectional chargers ignoring the influences of obstacles on the charging process. Similar to our WAIT scheme, after extracting the Dominating Coverage Sets and their corresponding subareas, WCP uses a greedy-based approach to select the  $M$  locations that maximizes charging utility from the candidate locations to place the chargers.

**RANDom charger placement (RAN)** algorithm is an algorithm for randomly placing omnidirectional chargers in the network.

#### 4.2 Performance Comparison

**4.2.1 Instance Illustration.** Figure 9 shows the solutions for all algorithms for an instance with 18 sensors located in the 20 m × 20 m square. We can see that the WAIT scheme tends to place one charger (e.g.,  $c_1, c_2$ ) around obstacles with low attenuation coefficient to charge multiple sensors on both sides of obstacles. In contrast, around metal obstacles, WAIT tends to place charger to charge each sensor within its proximity (e.g.,  $c_3, c_4, c_5$ ). The rationale behind this is that WAIT fully considers the different blocking impacts of the obstacles’ materials and thickness, then

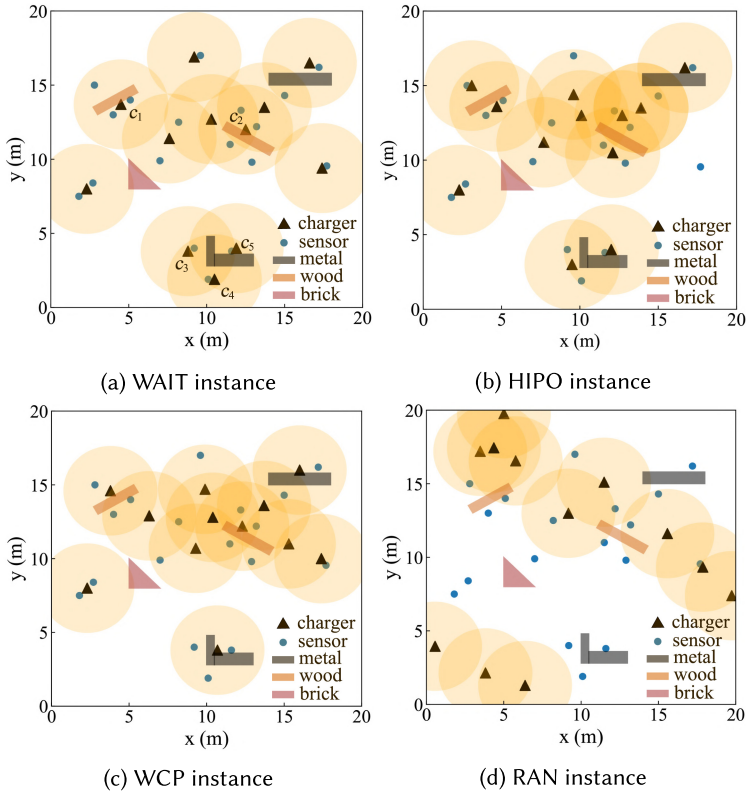


Fig. 9. Instances.

Table 3. Running Results of Different Algorithms

	WAIT	HIPO	WCP	RAN
Charging Utility	17.017	14.413	12.627	5.045

reasonably chooses the placement locations for chargers according to the location relationship between obstacles and sensors. The charging utility achieved by four algorithms in the default network environment are shown in Table 3.

It can be seen that the charging utility achieved by WAIT is much larger than HIPO, WCP, and RAN do. This means that our WAIT is suitable for practical charging scenario where multiple obstacles with different materials, shapes and sizes are distributed. The charging utility achieved by HIPO is 14.413, less than that achieved by WAIT. This indicates that the assumption that all obstacles can completely block electromagnetic waves does not hold in real applications. Moreover, since the WCP algorithm ignores the influences of obstacles on the propagation of electromagnetic waves, its charging utility is lower than that of WAIT and HIPO. The charging utility achieved by RAN is the smallest. The reason is that the placement locations for chargers are randomly selected.

**4.2.2 Impact of Number of Chargers  $M$ .** Our simulation results show that on average, WAIT outperforms HIPO, WCP, and RAN by 20.6%, 41.08%, and 248%, respectively, in terms of  $M$ . Figure 10(a) shows that the overall charging utility increases monotonically with  $M$ . Moreover,

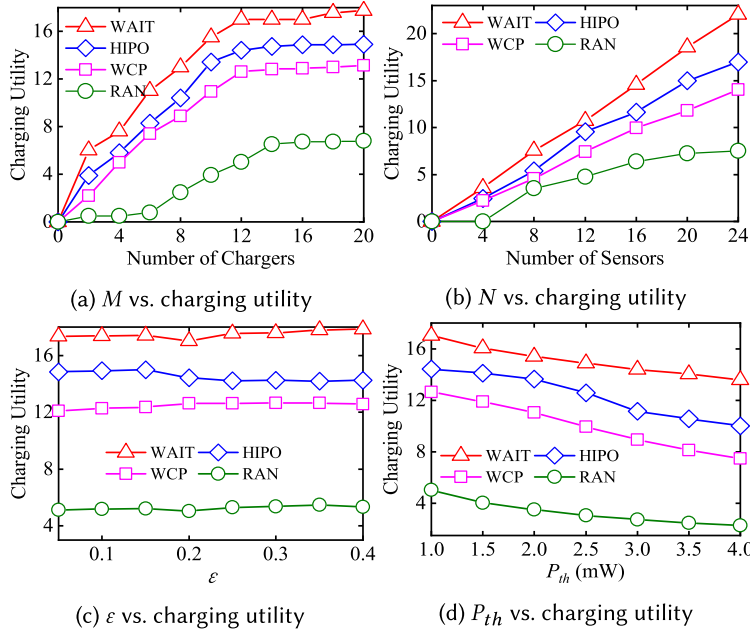


Fig. 10. Simulations.

the charging utility of our WAIT first increases at a high rate and then keeps relatively stable at 17 when  $M$  reaches 14. The essential reason for this trend is that our WAIT problem is submodular, which has been proved in Section 3.4. In contrast, although comparison algorithms have the same trend, the maximum charging utility achieved by these three algorithms are only 14.9, 13.14, and 6.8, respectively.

**4.2.3 Impact of Number of Sensors  $N$ .** Our simulation results show that on average, WAIT outperforms HIPO, WCP, and RAN by 26.3%, 53.8%, and 161.9%, respectively, in terms of  $N$ . From Figure 10(b), we can see that the charging utility of all algorithms increases monotonically with  $N$ . Note that, the performance of our WAIT scheme grows almost linearly with  $N$ . This indicates that WAIT can obtain stable charging utility from each sensor under different sensor densities. Furthermore, with the increase of  $N$ , the advantage of WAIT becomes more obvious, which further indicates that WAIT is more effective than the other three algorithms.

**4.2.4 Impact of Error Threshold  $\epsilon$ .** Our simulation results show that on average, WAIT outperforms HIPO, WCP, and RAN by 20.6%, 40.1%, and 232.6%, respectively, in terms of  $\epsilon$ . It can be seen from Figure 10(c), with the increase of  $\epsilon$ , the charging utility of all algorithms is all stable, and that of our WAIT scheme is always greater than 17. This suggests that we can reduce the running time of the WAIT algorithm without significant performance loss by setting a larger  $\epsilon$ .

**4.2.5 Impact of Power Threshold  $P_{th}$ .** Our simulation results show that on average, WAIT outperforms HIPO, WCP, and RAN by 21.8%, 50.5%, and 354.9%, respectively, in terms of  $P_{th}$ . As shown in Figure 10(d), the charging utility of all algorithms decreases slightly as  $P_{th}$  increases. This is because with the increase of  $P_{th}$ , the energy received by the sensor will gradually be less than  $P_{th}$ , which makes its charging utility smaller, resulting in the decline of the overall charging utility. Even so, our WAIT algorithm still outperforms other comparison algorithms.



Fig. 11. Testbed.

## 5 FIELD EXPERIMENTS

In this section, we conduct field experiments to verify the performance of the proposed WAIT scheme.

### 5.1 Experimental Setup

As shown in Figure 11, our testbed consists of eight sensors and three TX91501 wireless chargers (both of them are produced by Powercast [34]), which are placed on a  $4\text{ m} \times 3\text{ m}$  2D plane. Moreover, there are three obstacles of different shapes distributed on the plane, which are made of wood, bricks, and metal, respectively. The coordinates of eight sensors are  $(0.94, 1.28)$ ,  $(0.48, 0.52)$ ,  $(0.64, 2.22)$ ,  $(1.84, 0.82)$ ,  $(2.78, 1.64)$ ,  $(3.1, 2.2)$ ,  $(3.4, 1.54)$ , and  $(1.3, 1.96)$ , respectively. In addition, we set  $D = 1\text{m}$ ,  $P_{th} = 10\text{ mW}$ , and use Equation (2) to calculate the charging utility of each sensor. Since TX91501 is a directional charger, to migrate impacts given by orientation angles, we rotate it when necessary to mimic omnidirectional charger [7, 23, 27, 45]. Considering the randomness and uncertainty of the RAN algorithm, we use **Uniform Deployment Algorithm (UDA)** here to evenly distribute the three chargers in the network area. Note that, since a wireless charger will be deployed inside the obstacle when using the horizontal UDA algorithm, we apply the vertical UDA algorithm to deploy the wireless chargers and their coordinates are  $(2, 2.25)$ ,  $(2, 1.5)$ , and  $(2, 0.75)$ , respectively.

### 5.2 Experiments Results

In Figure 12, the placement schemes for WAIT, HIPO, WCP, and UDA are depicted in red, black, purple, and green, respectively. Table 4 gives the detailed placement coordinates of each charger generated by the four schemes. Figure 13 shows the charging utility obtained by each sensor. We can see that only our WAIT can achieve charging utility from all sensors. This means that all sensors can be covered by the chargers deployed by WAIT. Moreover, there are seven sensors that obtain the highest charging utility, which further verifies the effectiveness of our WAIT scheme significantly. The overall charging utility achieved by all algorithms is shown in Table 5. It can be seen that our WAIT scheme outperforms HIPO, WCP, and UDA by 23%, 43.4%, and 240.9%, respectively.

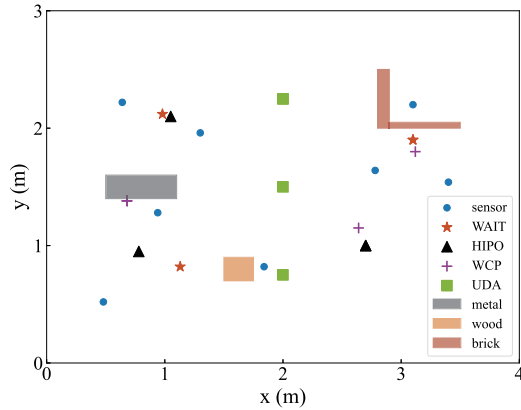


Fig. 12. Positions of chargers and sensors.

Table 4. Charger Placement Scheme for Four Algorithms in Field Experiment

chargerID	WAIT	HIPO	WCP	UDA
1	(3.1, 1.9)	(2.7, 1)	(0.68, 1.38)	(2, 2.25)
2	(1.13, 0.82)	(0.78, 0.95)	(2.64, 1.15)	(2, 1.5)
3	(0.98, 2.12)	(1.05, 2.1)	(3.12, 1.8)	(2, 0.75)

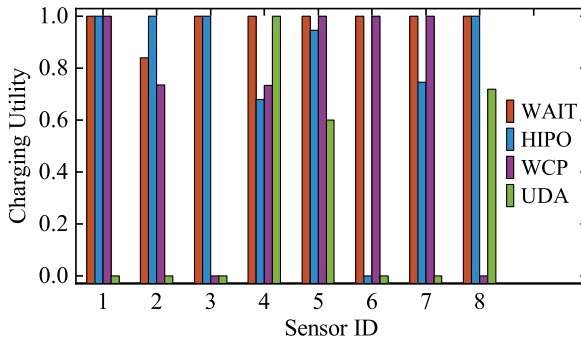


Fig. 13. Charging utility of each sensor.

Table 5. Overall Charging Utility for Four Algorithms in Field Experiment

	WAIT	HIPO	WCP	UDA
Charging Utility	7.84	6.373	5.469	2.3

## 6 DISCUSSION

**How to achieve a required charging utility by deploying the minimum number of chargers?**

Using the minimum number of chargers to obtain the required charging utility from all sensors is an NP hard problem, which can be proved by a reduction from the set cover problem [9]. It

is worth pointing out that different from the traditional set cover problem in wireless charging field, the coverage range of each charger may no longer be a standard circle due to obstacles. Nevertheless, we can still use the practical charging model with obstacles proposed in this article to get different sensors covered by different chargers. And then, all Dominating Coverage Sets and corresponding candidate subareas can be extracted by employing the proposed Dominating Coverage Sets extraction algorithm. Finally, we can revise our greedy algorithm to select candidate placement locations one by one, until the required charging utility is achieved. According to the analysis results in Reference [5], the greedy algorithm can achieve  $\frac{1}{\ln m}$  approximate ratio, where  $m$  is the number of candidate placement locations.

### **How to design an on-demand charging scheme to charge sensors in practical charging scenarios with obstacles wirelessly?**

The **Mobile Charger (MC)** scheduling is an important problem in wireless charging field. In the real scenario with obstacles, there are two critical problems when we design an effective charging scheduling scheme: (i) how to obtain sojourn areas for MC to cover sensors with charging demands by considering the influences of obstacles on electromagnetic waves; (ii) how to plan the charging order for the MC to visit these sojourn areas and generate the shortest charging path that can avoid obstacles.

For the first problem, similar to our WAIT scheme, the MC's placeable area of each sensor with charging demand can be easily obtained by using our practical charging model with obstacles. Then, we can design an approximation algorithm to find the minimum number of overlapping areas that can cover all sensors from all overlapping areas formed by these placeable areas. For the second problem, a feasible method is to determine the charging order for the MC to visit these sojourn areas according to the residual lifetimes of sensors. Then, we can design a charging location selection algorithm for MC to select a charging location from each sojourn area to generate the shortest charging path. Furthermore, if there are obstacles on the charging path, the **Obstacle Avoidance (OA)** algorithm proposed in Reference [2] can be used to adjust the charging path.

## **7 RELATED WORK**

In recent years, much effort has been devoted to constructing WRSNs. Generally, previous studies can be classified into two categories based on the different functionalities of wireless chargers: wireless charger placement [9, 10, 32, 42, 47, 50] and mobile charger scheduling [19, 23–25, 30, 35, 37, 45].

### **7.1 Wireless charger placement**

For the wireless charger placement issue, the stationary chargers transmit energy to surrounding sensors within the charging range. Zhang et al. [50] studied the joint optimization problem of charger placement and power allocation to maximize the charging quality, subject to a power budget. Dai et al. [9] focused on how to optimize the charging utility by using directional wireless chargers. The authors developed an approximation algorithm to obtain the placement locations and the orientations for chargers. In Reference [10], Dai et al. also proposed a wireless charger placement scheme with limited mobility and further designed an approximate algorithm to maximize the overall charging utility. Yu et al. [47] first considered the wireless charger placement problem under connectivity constraint for wireless chargers, and then they proposed a constant approximation algorithm to determine the placement position and orientation angle for each charger. Note that the above traditional studies all ignored the impacts of obstacles, making these schemes unsuitable for practical charging scenarios. Ma et al. [32] considered the wave interference in the concurrent charging scenario and they proposed a concurrent charging

scheme to take full advantage of the high power caused by constructive interference to enhance the charging efficiency. Recently, Wang et al. [42] considered the wireless charger placement with obstacles for the first time. However, they assumed that the electromagnetic waves cannot penetrate any obstacles, which conflicts with the real environment.

## 7.2 Mobile Charger Scheduling

For the mobile charger scheduling issue, mobile chargers are introduced to visit energy-critical sensors in some order to replenish energy to them. Liu et al. [30] proposed a partial charging scheme to jointly optimize the number of dead sensors and the energy usage effectiveness. Different from the traditional 2D scheduling, Lin et al. [25] employed drone as the mobile charger to replenish energy to sensors in 3D scenarios. They developed a cost-efficient algorithm to maximize the energy received by all sensors, which is subject to the energy budget of the drone. In Reference [19], Jia et al. designed a computational geometry-based algorithm to select multiple charging positions where the mobile charger stays to charge nearby sensors. Yang et al. [45] studied the mobile charger scheduling problem for multi-sensor recharging with deadline constraints to maximize the overall effective charging utility and minimize the travelling time for moving as well. Tomar et al. [37] proposed a novel scheduling scheme for on-demand charging scenario. They have adopted the Mamdani Fuzzy Inference System to determine the charging order for the sensors. Ren et al. [35] exploited the neglected back lobe for mobile charging to jointly minimize the number of dead sensors and maximize energy usage efficiency. Different from the above researches, which neglected the existence of obstacles, Lin et al. [23, 24] concentrated on maximizing charging utility in a practical WRSNs with obstacles. They first proposed a charging model based on the Fresnel diffraction model by transforming obstacles into equivalent screens. Afterwards, they designed a scheduling algorithm to generate a charging path for MC. However, this charging model is only applicable to metal obstacles with appropriate size (that is, the size of the obstacles is not greater than the wavelength), so the applicability of this model in practical scenarios is quite limited.

## 8 CONCLUSION

In this work, we focus on how to design a practical charger placement scheme for WRSNs with obstacles. To obtain the energy strength of the areas blocked by obstacles, we first jointly consider the influences of the material, size, and position of obstacles on electromagnetic wave propagation to build a practical charging model with obstacles based on shadow fading. We also conduct testbed experiments to verify the correctness of this model. Further, we design a piecewise constant function to approximate nonlinear charging power and propose a Dominating Coverage Set extraction algorithm to reduce the continuous solution space to a limited number. Then, we develop a greedy algorithm to select the appropriate placement location for each charger. Finally, we carry out extensive simulations and testbed experiments to show that our proposed scheme outperforms the state-of-the-art work.

In this article, our primary goal is to investigate the impact of obstacles on the propagation of charging signals in practical charging scenarios. Thus, to simplify the charging model with obstacles, we adopt the settings proposed in References [6, 8, 17, 41, 48, 49]. These settings assume the energy received by a sensor from multiple chargers is additive. Although the effectiveness of this assumption has been proven in low-density WRSNs, it is important to consider the influence of wave interference in high-density networks, which can result in complex energy distribution [16, 32]. Thus, in future, we will focus on how to design a more efficient and practical charger placement scheme for high-density WRSNs with obstacles.

## REFERENCES

- [1] Goldsmith Andrea. 2017. *Wireless Communication*.
- [2] Luitpold Babel. 2017. Curvature-constrained traveling salesman tours for aerial surveillance in scenarios with obstacles. *Eur. J. Oper. Res.* 262, 1 (2017), 335–346.
- [3] J. E. Berg, Randall Bownds, and Fredrik Lotse. 1992. Path loss and fading models for microcells at 900 MHz. In *Proceedings of the IEEE VTC*. 666–671.
- [4] David Keun Cheng et al. 1989. *Field and Wave Electromagnetics*. Pearson Education India.
- [5] Vasek Chvatal. 1979. A greedy heuristic for the set-covering problem. *Math. Oper. Res.* 4, 3 (1979), 233–235.
- [6] Haipeng Dai, Yunhuai Liu, Guihai Chen, Xiaobing Wu, Tian He, Alex X. Liu, and Huizhen Ma. 2017. Safe charging for wireless power transfer. *IEEE/ACM Trans. Netw.* 25, 6 (2017), 3531–3544.
- [7] Haipeng Dai, Yunhuai Liu, Nan Yu, Chaofeng Wu, Guihai Chen, Tian He, and Alex X. Liu. 2021. Radiation constrained wireless charger placement. *IEEE/ACM Trans. Netw.* 29, 1 (2021), 48–64.
- [8] Haipeng Dai, Huizhen Ma, and Alex X. Liu. 2017. Radiation constrained scheduling of wireless charging tasks. In *Proceedings of the ACM MobiHoc*. 1–10.
- [9] Haipeng Dai, Xiaoyu Wang, Alex X. Liu, Huizhen Ma, and Guihai Chen. 2017. Optimizing wireless charger placement for directional charging. In *Proceedings of the IEEE INFOCOM*. 1–9.
- [10] Haipeng Dai, Chaofeng Wu, Xiaoyu Wang, Wanchun Dou, and Yunhuai Liu. 2020. Placing wireless chargers with limited mobility. In *Proceedings of the IEEE INFOCOM*. 2056–2065.
- [11] Vinko Erceg, Larry J. Greenstein, Sony Y. Tjandra, Seth R. Parkoff, Ajay Gupta, Boris Kulic, Arthur A. Julius, and Renee Bianchi. 1999. An empirically based path loss model for wireless channels in suburban environments. *IEEE J. Select. Areas Commun.* 17, 7 (1999), 1205–1211.
- [12] Xiaoran Fan, Longfei Shangguan, Richard Howard, Yanyong Zhang, Yao Peng, Jie Xiong, Yunfei Ma, and XiangYang Li. 2020. Towards flexible wireless charging for medical implants using distributed antenna system. In *Proceedings of the ACM MobiCom*. 1–15.
- [13] Chao Feng, Jie Xiong, Liqiong Chang, Ju Wang, Xiaojiang Chen, Dingyi Fang, and Zhanyong Tang. 2019. Wimi: Target material identification with commodity Wi-Fi devices. In *Proceedings of the IEEE ICDCS*. 700–710.
- [14] Satoru Fujishige. 2005. *Submodular Functions and Optimization*. Elsevier.
- [15] Andrea J. Goldsmith and Larry J. Greenstein. 1993. A measurement-based model for predicting coverage areas of urban microcells. *IEEE J. Select. Areas Commun.* 11, 7 (1993), 1013–1023.
- [16] Peng Guo, Xuefeng Liu, Shaojie Tang, and Jiannong Cao. 2017. Concurrently wireless charging sensor networks with efficient scheduling. *IEEE Trans. Mobile Comput.* 16, 9 (2017), 2450–2463.
- [17] Shibo He, Jiming Chen, Fachang Jiang, David K. Y. Yau, Guoliang Xing, and Youxian Sun. 2013. Energy provisioning in wireless rechargeable sensor networks. *IEEE Trans. Mobile Comput.* 12, 10 (2013), 1931–1942.
- [18] Wenjie Huang, Zhiwei Zhao, Zi Wang, Geyong Min, Zheng Chang, Luwei Fu, and Hancong Duan. 2023. Adaptive mobile recharge scheduling with rapid data sharing in wireless rechargeable networks. *IEEE Trans. Mobile Comput.* (2023).
- [19] Riheng Jia, Jinhao Wu, Jianfeng Lu, Minglu Li, Feilong Lin, and Zhonglong Zheng. 2022. Energy saving in heterogeneous wireless rechargeable sensor networks. In *Proceedings of the IEEE INFOCOM*. 1838–1847.
- [20] Andre Kurs, Aristeidis Karalis, Robert Moffatt, John D. Joannopoulos, Peter Fisher, and Marin Soljacic. 2007. Wireless power transfer via strongly coupled magnetic resonances. *Science* 317, 5834 (2007), 83–86.
- [21] Eun S. Lee, Yeong H. Sohn, Byeong G. Choi, Seung H. Han, and Chun T. Rim. 2018. A modularized IPT with magnetic shielding for a wide-range ubiquitous Wi-power zone. *IEEE Trans. Power Electron.* 33, 11 (2018), 9669–9690.
- [22] Lanlan Li, Haipeng Dai, Guihai Chen, Jiaqi Zheng, Wanchun Dou, and Xiaobing Wu. 2019. Radiation constrained fair charging for wireless power transfer. *ACM Trans. Sensor Netw.* 15, 2 (2019), 1–33.
- [23] Chi Lin, Feng Gao, Haipeng Dai, Jiankang Ren, Lei Wang, and Guowei Wu. 2020. Maximizing charging utility with obstacles through Fresnel diffraction model. In *Proceedings of the IEEE INFOCOM*. 2046–2055.
- [24] Chi Lin, Feng Gao, Haipeng Dai, Lei Wang, and Guowei Wu. 2019. When wireless charging meets fresnel zones: Even obstacles can enhance charging efficiency. In *Proceedings of the IEEE SECON*. 1–9.
- [25] Chi Lin, Wei Yang, Haipeng Dai, Teng Li, Yi Wang, Lei Wang, Guowei Wu, and Qiang Zhang. 2021. Near optimal charging schedule for 3-D wireless rechargeable sensor networks. *IEEE Trans. Mobile Comput.* (2021).
- [26] Chi Lin, Ziwei Yang, Haipeng Dai, Liangxian Cui, Lei Wang, and Guowei Wu. 2021. Minimizing charging delay for directional charging. *IEEE/ACM Trans. Netw.* 29, 6 (2021), 2478–2493.
- [27] Chi Lin, Ziwei Yang, Jiankang Ren, Lei Wang, Wei Zhong, Guowei Wu, and Qiang Zhang. 2022. Are you really charging me? In *Proceedings of the IEEE ICDCS*. 724–734.
- [28] Jingxiang Liu, Jian Peng, Wenzheng Xu, Weifa Liang, Tang Liu, Xi Peng, Zichuan Xu, Zheng Li, and Xiaohua Jia. 2022. Maximizing sensor lifetime via multi-node partial-charging on sensors. *IEEE Trans. Mobile Comput.* (2022).

- [29] Tang Liu, Baijun Wu, Wenzheng Xu, Xianbo Cao, Jian Peng, and Hongyi Wu. 2021. RLC: A reinforcement learning-based charging algorithm for mobile devices. *ACM Trans. Sensor Netw.* 17, 4 (2021), 1–23.
- [30] Tang Liu, Baijun Wu, Shihao Zhang, Jian Peng, and Wenzheng Xu. 2020. An effective multi-node charging scheme for wireless rechargeable sensor networks. In *Proceedings of the IEEE INFOCOM*. 2026–2035.
- [31] Zhihong Luo, Qiping Zhang, Yunfei Ma, Manish Singh, and Fadel Adib. 2019. 3D backscatter localization for fine-grained robotics. In *Proceedings of the USENIX NSDI*. 765–782.
- [32] Yuzhuo Ma, Die Wu, Meixuan Ren, Jian Peng, Jilin Yang, and Tang Liu. 2023. Concurrent charging with wave interference. In *Proceedings of the IEEE INFOCOM*.
- [33] Yasamin Mostofi, Alejandro Gonzalez-Ruiz, Alireza Gaffarkhah, and Ding Li. 2009. Characterization and modeling of wireless channels for networked robotic and control systems-a comprehensive overview. In *Proceedings of the IEEE IROS*. 4849–4854.
- [34] Powercast. Retrieved from <http://www.powercastco.com>
- [35] Meixuan Ren, Die Wu, Jing Xue, Wenzheng Xu, Jian Peng, and Tang Liu. 2023. Utilizing the neglected back lobe for mobile charging. In *Proceedings of the IEEE INFOCOM*.
- [36] Yu Sun, Chi Lin, Haipeng Dai, Pengfei Wang, Lei Wang, Guowei Wu, and Qiang Zhang. 2022. Trading off charging and sensing for stochastic events monitoring in WRSNs. *IEEE/ACM Trans. Netw.* 30, 2 (2022), 557–571.
- [37] Abhinav Tomar, Lalatendu Muduli, and Prasanta K. Jana. 2021. A fuzzy logic-based on-demand charging algorithm for wireless rechargeable sensor networks with multiple chargers. *IEEE Trans. Mobile Comput.* 20, 9 (2021), 2715–2727.
- [38] Deepak Vasisht, Swaran Kumar, and Dina Katabi. 2016. Decimeter-level localization with a single WiFi access point. In *Proceedings of the USENIX NSDI*. 165–178.
- [39] Ju Wang, Jie Xiong, Xiaojiang Chen, Hongbo Jiang, Rajesh Krishna Balan, and Dingyi Fang. 2021. Simultaneous material identification and target imaging with commodity RFID devices. *IEEE Trans. Mobile Comput.* 20, 2 (2021), 739–753.
- [40] Ning Wang, Jie Wu, and Haipeng Dai. 2019. Bundle charging: Wireless charging energy minimization in dense wireless sensor networks. In *Proceedings of the IEEE ICDCS*. IEEE, 810–820.
- [41] Xiaoyu Wang, Haipeng Dai, He Huang, Yunhuai Liu, Guihai Chen, and Wanchun Dou. 2019. Robust scheduling for wireless charger networks. In *Proceedings of the IEEE INFOCOM*. 2323–2331.
- [42] Xiaoyu Wang, Haipeng Dai, Weijun Wang, Jiaqi Zheng, Nan Yu, Guihai Chen, Wanchun Dou, and Xiaobing Wu. 2020. Practical heterogeneous wireless charger placement with obstacles. *IEEE Trans. Mobile Comput.* 19, 8 (2020), 1910–1927.
- [43] Bin Xiao, Jiannong Cao, Qingfeng Zhuge, Yi He, and E. H. M. Sha. 2004. Approximation algorithms design for disk partial covering problem. In *Proceedings of the IEEE ISSPAN*. 104–109.
- [44] Wenzheng Xu, Weifa Liang, Zichuan Xu, Jian Peng, Dezhong Peng, Tang Liu, Xiaohua Jia, and Sajal K. Das. 2021. Approximation algorithms for the generalized team orienteering problem and its applications. *IEEE/ACM Trans. Netw.* 29, 1 (2021), 176–189.
- [45] Panlong Yang, Tao Wu, Haipeng Dai, Xunpeng Rao, Xiaoyu Wang, Peng-Jun Wan, and Xin He. 2020. MORE: Multi-node mobile charging scheduling for deadline constraints. *ACM Trans. Sensor Netw.* 17, 1 (2020), 1–21.
- [46] Yuanyuan Yang and Cong Wang. 2015. *Wireless Rechargeable Sensor Networks*. Springer.
- [47] Nan Yu, Haipeng Dai, Guihai Chen, Alex X. Liu, Bingchuan Tian, and Tian He. 2021. Connectivity-constrained placement of wireless chargers. *IEEE Trans. Mobile Comput.* 20, 3 (2021), 909–927.
- [48] Jin Zhang, Hong Gao, Quan Chen, and Jianzhong Li. 2023. Task-oriented energy scheduling in wireless rechargeable sensor networks. *ACM Trans. Sensor Netw.* 19, 4 (2023), 1–32.
- [49] Sheng Zhang, Zhuzhong Qian, Fanyu Kong, Jie Wu, and Sanglu Lu. 2015. P3: Joint optimization of charger placement and power allocation for wireless power transfer. In *Proceedings of the IEEE INFOCOM*. IEEE, 2344–2352.
- [50] Sheng Zhang, Zhuzhong Qian, Jie Wu, Fanyu Kong, and Sanglu Lu. 2018. Wireless charger placement and power allocation for maximizing charging quality. *IEEE Trans. Mobile Comput.* 17, 6 (2018), 1483–1496.

Received 18 January 2023; revised 28 May 2023; accepted 31 July 2023